Int J Fract (2010) 164:231–252
DOI 10.1007/s10704-010-9488-3

ORIGINAL PAPER

An engineering methodology to assess effects of weld strength mismatch on cleavage fracture toughness using the Weibull stress approach

Claudio Ruggieri

Received: 31 July 2009 / Accepted: 30 March 2010 / Published online: 23 April 2010

Abstract This work describes the development of an engineering approach based upon a toughness scaling methodology incorporating the effects of weld strength mismatch on crack-tip driving forces. The approach adopts a nondimensional Weibull stress, $\bar{\sigma}_w$, as a the near-tip driving force to correlate cleavage fracture across cracked weld configurations with different mismatch conditions even though the loading parameter (measured by J) may vary widely due to mismatch and constraint variations. Application of the procedure to predict the failure strain for an overmatch girth weld made of an API X80 pipeline steel demonstrates the effectiveness of the micromechanics approach. Overall, the results lend strong support to use a Weibull stress based procedure in defect assessments of structural welds.

Keywords Cleavage fracture · Local approach · Weibull stress · Weld · Strength mismatch

1 Introduction

Structural integrity assessments of steel weldments remain a key issue in design, fabrication and safe operation of critical engineering structures, including pressure vessels and storage tanks, piping systems, submarine hulls and offshore oil structures among others. Typical welding processes introduce strong thermal cycles and inhomogeneous cooling in the weld metal and surrounding region (including the heat affected zone—HAZ) which often deteriorate the metallurgical quality and potentially lower the inherent fracture toughness of the weldment (Kerr 1976). The reduced fracture performance of the weld joint (as compared with the baseplate material) largely increases the likelihood of failure at an undetected crack-like defect in the welded region, most often in the form of planar flaws (e.g., hot or cold cracking, lack of penetration, undercut) (American Welding Society 1987; Jutla 1996; Glover et al. 1986). To reduce the likelihood of structural failure caused by a weld defect or weld flaw formed during operation, many codes and current fabrication practices (see American Society of Mechanical Engineers 2004; American Petroleum Institute 2005; Det Norske Veritas 2007 for illustrative examples) require the use of weldments with weld metal strength higher than the baseplate strength; a condition referred to as overmatching. An evident benefit and primary motivation to use weld overmatching is to limit the higher stresses that would otherwise occur in a homogeneous material thereby shielding the welded region. Moreover, the overmatch weld also causes the large plastic deformation field to shift into the lower strength baseplate where the fracture resistance is presumably higher and potentially fewer defects occur.

C. Ruggieri (✉)
Department of Naval Architecture and Ocean Engineering, University of São Paulo, São Paulo, SP 05508-900, Brazil
e-mail: claudio.ruggieri@usp.br

While the overmatch practice has been used effectively in many structural applications, the level of mismatch between the weld metal and baseplate material may strongly alter the relationship between remotely applied loading and crack-tip driving forces, such as the J-integral and its corresponding value of the Crack Tip Opening Displacement, CTOD or δ (Anderson 2005). The interaction between the local crack-tip fields (most often controlled by the flow properties of the weld metal) and the global elastic-plastic regime gives rise to near-tip constraint states which can differ significantly than the corresponding levels in crack-tip constraint for a homogeneous fracture specimen at the same (macroscopic) loading. Such features introduce additional difficulties in fracture mechanics based approaches (such as, for example, BS7910 (2005) and API 579 (2007a)) defining defect acceptance criteria for welded components based upon macroscopic measures of cleavage fracture toughness (J_c or δ_c). Moreover, cleavage fracture is a highly localized failure mechanism which is strongly dependent on material characteristics at the microlevel. In particular, the random inhomogeneity in local features of the material causes large scatter in experimentally measured values of fracture toughness in the ductile-to-brittle transition (DBT) region. This phenomenon is further magnified by the overmatching condition in steel weldments thereby contributing to potentially increase the propensity to trigger cleavage before gross yield section. Clearly, the transferability of fracture toughness data measured using small, laboratory specimens to large, complex structural components still remains one of the key difficulties in developments of predictive methodologies for defect assessments of welded structures. Advanced procedures for structural integrity analyses must include the complex interplay between the effects of weld strength mismatch and the variability of cleavage resistance at the microstructural level for the different regions of steel weldments.

The synergic effects of strength mismatch and scatter of toughness values in the DBT region motivate the introduction of a micromechanics model capable of coupling macroscopic measures of fracture toughness with local failure conditions. In particular, the seminal work of Beremin (1983) provides the basis for establishing a relationship between the microregime of fracture and macroscopic crack driving forces (such as the J-integral) by introducing the Weibull stress (σ_w) as a probabilistic fracture parameter. A key feature of the Beremin approach is that σ_w follows a Weibull distribution (Weibull 1939; Mann et al. 1974) in terms of the Weibull modulus, m, and the scale parameter, σ_u. When implemented in a finite element code, the Beremin model predicts the evolution of the Weibull stress with applied (macroscopic) load to define conditions leading to (local) material failure. Previous research efforts to develop a transferability model to elastic-plastic fracture toughness values rely on the notion of the Weibull stress as a crack-tip driving force (Ruggieri and Dodds 1996a,b; Ruggieri 2001, 2009a). The central feature in this methodology adopts the simple axiom that unstable crack propagation (cleavage) occurs at a critical value of the Weibull stress; under increased remote loading (as measured by J or CTOD), differences in evolution of the Weibull stress reflect the potentially strong variations of near-tip stress fields and crack-tip constraint. However, further developments of the Weibull stress approach to include effects of weld strength mismatch remain rather untested, as does its extension into simpler procedures to transfer fracture toughness data measured using small, welded specimens to large, complex welded components. Such procedures require a robust and yet simplified methodology reflecting the strong role of strength mismatch and statistical variability on correlations of toughness data for varying crack configurations and loading modes (tension vs. bending).

This work describes an engineering methodology incorporating the statistics of microcracks and a probability distribution of the (local) fracture stress to assess the effects of weld strength mismatch on crack-tip driving forces. One purpose of this investigation is to extend the framework for structural integrity assessments building upon a local fracture parameter, here characterized by the Weibull stress (σ_w), to welded components. Another purpose is to assess the effectiveness of a toughness scaling model based upon a nondimensional interpretation of σ_w in integrity analyses of welded components with varying mismatch conditions. Fracture testing of girth welds obtained from an API X80 pipeline steel provide the data needed to validate the proposed methodology in failure predictions. Such an application serves as a prototype for a wide class of integrity assessment problems involving the effects of weld strength mismatch on fracture toughness values. Overall, the results lend additional support to use a Weibull stress based procedures in defect assessments of structural welds.

2 The Weibull stress model for strength mismatched welds

The objectives in developing probabilistic models to describe unstable crack propagation are essentially two fold. First, for a structure containing cracks of different sizes and subjected to complex loading histories, a probability distribution for the (local) fracture stress is sought to couple the remote loading (as measured by J or CTOD) with the operative (cleavage) fracture mechanism at the microlevel. In the context of probabilistic models, a fracture parameter associated with the probability distribution then describes macroscopic fracture behavior for a wide range of loading conditions and crack configurations. As a second objective, prediction of unstable crack propagation in larger flawed structures can be made on the basis of a probabilistic fracture parameter. Experimentally measured values of fracture toughness for one configuration (e.g., small laboratory specimens for homogeneous materials and weldments) are rationally extended to predict unstable crack propagation for other crack configurations, including welded components, provided similarities in both probability distributions for such fracture parameter exist.

This section provides the essential features of the theoretical framework needed to introduce a transferability model for elastic-plastic fracture toughness values in strength mismatched welds based upon the Weibull stress approach. The description that follows draws heavily on the early work of Beremin (1983) and Ruggieri and Dodds (1996a,b), Ruggieri (2001, 2009a). A summary of the probabilistic approach upon which the Weibull stress is derived sets the necessary framework to define a nondimensional σ_w incorporating effects of weld strength mismatch. Subsequent development focuses on a simpler extension of the toughness scaling methodology for cracked welded configurations with different levels of strength mismatch.

2.1 Overview of probabilistic modeling for cleavage fracture in ferritic steels

Laboratory testing of ferritic steels in the ductile-to-brittle (DBT) region consistently reveals a marked scatter in the measured values of cleavage fracture toughness. Extreme value statistics (Mann et al. 1974) provide a formal framework to describe the macroscopic variability in cleavage fracture data. A continuous probability function derived from a weakest link interpretation of the cleavage fracture process conveniently characterizes the distribution of toughness values in the form (Weibull 1939; Mann et al. 1974)

$$F(J_c) = 1 - \exp\left[-\left(\frac{J_c - J_{\min}}{J_0 - J_{\min}}\right)^{\alpha}\right] \tag{1}$$

which is a three-parameter Weibull distribution with parameters (α, J_0, $J_{\min}$). Here, α denotes the Weibull modulus (shape parameter), J_0 defines the characteristic toughness (scale parameter) and $J_{\min}$ is the threshold fracture toughness. A number of statistical models for transgranular cleavage fracture have been derived based upon the adoption of a three-parameter Weibull function either based upon a threshold fracture strength (Evans and Langdon 1976; Matsuo 1981; Lin et al. 1986) or a threshold fracture toughness (Ruggieri 2001; Wallin 1984, 2002; American Society for Testing and Materials 2008b).

Because accurate and reliable estimates of $J_{\min}$ are not always warranted, the threshold fracture toughness is often set equal to zero so that the Weibull function given by Eq. (1) assumes its more familiar and widely adopted, albeit somewhat conservative, two-parameter form

$$F(J_c) = 1 - \exp\left[-\left(\frac{J_c}{J_0}\right)^{\alpha}\right] \tag{2}$$

The above probability distribution remains applicable for other measures of fracture toughness, such as K_{Jc} or CTOD. A central feature emerging from this model is that, under SSY conditions, the scatter in cleavage fracture toughness data is characterized by $\alpha = 2$ for J_c-distributions (Minami et al. 1992) or $\alpha = 4$ for K_{Jc}-distributions (Wallin 1984, 2002; American Society for Testing and Materials 2008b).

Current probabilistic models to extend the previous statistical model given by Eq. (2) to multiaxially stressed, 3-D crack configurations employ weakest link arguments incorporating local criteria to couple the micromechanical features of the fracture process (such as the inherent random nature of cleavage fracture) with the inhomogeneous character of the near-tip stress fields. Figure 1a illustrates the fracture process zone ahead of the crack tip which is defined as the highly stressed region where the local operative mechanism for cleavage takes place; this region contains the potential sites for cleavage cracking. The overall fracture resistance is thus controlled by the largest

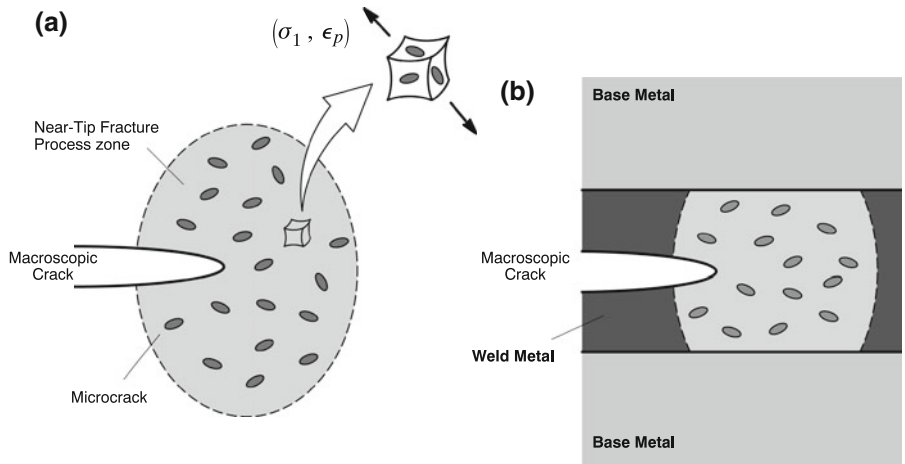

Fig. 1 **a** Near-tip fracture process zone ahead a macroscopic crack containing randomly distributed flaws; **b** Schematic of fracture process zone for a macroscopic crack embedded in the weld metal

fracture-triggering particle that is sampled in the fracture process zone ahead of crack front. Introduction of the Weibull stress (σ_w), a term coined by the Beremin (1983) group, provides the basis for generalizing the concept of a probabilistic fracture parameter and supports the development of procedures that unify toughness measures across different crack configurations and loading modes. The approach can be further extended to include the strong effects of near-tip plastic strain on cleavage microcracking thereby altering the microcrack distribution entering into the local criterion for fracture. Based upon direct observations of cleavage microcracking by plastic strain made in ferritic steels at varying temperatures (Brindley 1970; Lindley et al. 1970; Gurland 1972), the probability distribution for the fracture stress of a cracked solid with increased levels of loading (represented by the J-integral) can be defined by a two-parameter Weibull distribution (Beremin 1983; Ruggieri and Dodds 1996a,b; Ruggieri 2001, 2009a) with parameters m and σ_u in the form

$$F\left(\sigma_1\right) = 1 - \exp\left[-\frac{1}{\Omega_0}\int\limits_{\Omega} \varepsilon_p^{\gamma(1+\beta)}\left(\frac{\sigma_1}{\sigma_u}\right)^m d\Omega\right] \quad (3)$$

where Ω denotes the volume of the (near-tip) fracture process zone, Ω_0 is a reference volume and $\sigma_1 = f\left(J\right)$ is the maximum principal stress acting on material points inside the fracture process zone defined by the loci $\sigma_1 \geq \lambda\sigma_{ys}$, where $\lambda \approx 2$ and σ_{ys} is the material's yield stress. The plastic strain term appearing inside the integral of Eq. (3) derives from the dependence of the microcrack density on plastic deformation as shown in the Appendix. Here, $\varepsilon_p = h\left(J\right)$ is the near-tip effective plastic strain, γ and β are parameters defining the contribution of the plastic strain on cleavage fracture probability; for example, setting $\gamma = 0$ recovers the conventional description for the probability distribution of fracture stress (Ruggieri and Dodds 1996a,b; Ruggieri 2001, 2009a). The above plastic term correction simply reflects the increase in cleavage fracture probability that results from the raising in microcrack density with increased levels of near-tip plastic strain.

Now, following Beremin (1983), the Weibull stress, σ_w, is defined as the stress integral

$$\sigma_w = \left[\frac{1}{\Omega_0}\int\limits_{\Omega} \varepsilon_p^{\gamma(1+\beta)}\sigma_1^m d\Omega\right]^{1/m} \quad (4)$$

so that Eq. (3) is recast in the usual form

$$F\left(\sigma_w\right) = 1 - \exp\left[-\left(\frac{\sigma_w}{\sigma_u}\right)^m\right] \quad (5)$$

where parameter m most often takes a value in the range 10–22 for typical structural steels (Beremin 1983; Ruggieri and Dodds 1996a,b; Ruggieri 2001, 2009a; Bakker and Koers 1991; Gao et al. 1998; Ruggieri et al. 2000; Gao et al. 1999). To make contact with previously developed probabilistic models adopting the σ_w concept and to aid development of the scaling model described next, the above Eq. (4) can be interpreted as a generalized Weibull stress incorporating the effects of near-tip plastic strain. The Appendix provides further details on the development of the probabilistic modeling for cleavage fracture previously outlined.

In a related approach to predict constraint effects on cleavage fracture based upon the Weibull stress concept, Gao et al. (1998, 1999) have introduced a threshold Weibull stress directly into previous Eq. (5),

denoted as $\sigma_{w-\min}$, such as the failure probability for the cracked solid becomes zero for any σ_w-value below $\sigma_{w-\min}$. However, while initial applications of this approach have proven successful in cleavage fracture predictions of fracture specimens, there is no clear theoretical connection between the threshold fracture toughness, $J_{\min}$, appearing in Eq. (1) and the threshold Weibull stress, $\sigma_{w-\min}$. Ruggieri (2001) discusses this issue in detail and shows the minor role played by the use of threshold parameters in fracture predictions of conventional fracture specimens. Consequently, the present work adopts the same philosophy and proceeds with the analyses based upon a two-parameter Weibull function.

2.2 Toughness scaling methodology incorporating mismatch effects

Ruggieri and Dodds (1996a) proposed a toughness scaling model (TSM) based upon the Weibull stress approach to assess the effects of constraint variations on cleavage fracture toughness data. The present framework adopts the same philosophy but utilizes the concept of a nondimensional Weibull stress, hereafter denoted $\bar{\sigma}_w$, which is defined as σ_w normalized by the yield stress of the material where fracture takes place. To facilitate development of the TSM incorporating effects of weld strength mismatch, it proves convenient to first define the mismatch ratio, M_y, as

$$M_y = \frac{\sigma_{ys}^{WM}}{\sigma_{ys}^{BM}} \tag{6}$$

where σ_{ys}^{BM} and σ_{ys}^{WM} denote the yield stress for the base metal and weld metal. Based upon the interpretation of the generalized σ_w given by Eq. (4) as the crack-tip driving force, it follows that the nondimensional Weibull stress for a bimaterial system such as a welded joint can be defined as

$$\bar{\sigma}_w^k = \frac{\sigma_w^k}{\sigma_{ys}^k} \tag{7}$$

where $k = 1, 2$ corresponds to the baseplate and weld material. In adopting such nondimensional form for the Weibull stress, it is important to emphasize that the integration appearing in Eq. (4) must be performed over the volume of the fracture process zone for each material as depicted in Fig. 1b. With the Weibull stress defined in this manner, material points outside the region over which the integration is carried out are (implicitly) assigned a zero probability of cleavage fracture.

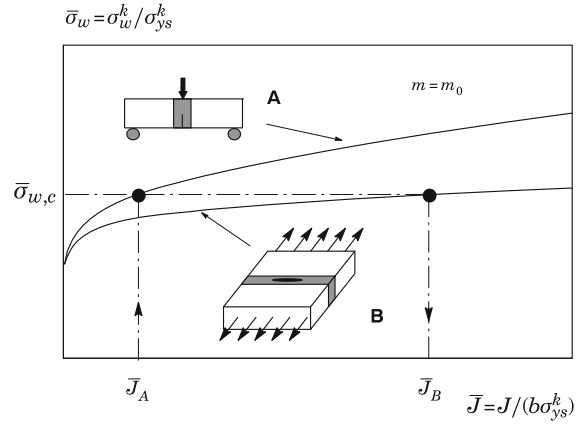

Fig. 2 Scaling procedure based on the normalized Weibull stress to correct toughness values for different crack configurations and mismatch conditions

Consider now extension of the TSM for toughness correlations in welded components. Based upon micromechanics considerations outlined previously, the proposed scaling model requires the attainment of a specified value for the nondimensional Weibull stress, $\bar{\sigma}_{w,c}$, to trigger cleavage fracture in different welded specimens subjected to different levels of crack-tip loading. Figure 2 illustrates the procedure to assess the effects of strength mismatch on cleavage fracture behavior needed to scale toughness values for cracked configurations with different mismatch conditions based upon the TSM strategy. The procedure employs a nondimensional crack driving force defined by $\bar{J} = J/\left(b\sigma_{ys}^k\right)$ where b is the remaining crack ligament as the measure of macroscopic loading, but remains valid for other measures of remote loading, such as CTOD. Without loss of generality, Fig. 2 displays $\bar{\sigma}_w$ versus $\bar{J}$ curves for a high constraint, welded configuration (such as a deep notch SE(B) specimen with a center-cracked square groove) made with an evenmatch condition ($M_y = 1$), denoted as configuration **A**, and a welded structural component (such as a surface crack specimen under tension loading) made with an overmatch condition ($M_y > 1$), denoted as configuration **B**. Very detailed, nonlinear 3-D finite element analyses provide the functional relationship between the Weibull stress ($\bar{\sigma}_w$) and applied loading ($\bar{J}$) for a specified value of the Weibull modulus, m_0. Given a measured toughness value at cleavage for the

high constraint, evenmatch fracture specimen ($\bar{J}_A$), the lines shown on Fig. 2 readily illustrate the technique used to determine the corresponding $\bar{J}_B$-value for the structural welded component.

A key assumption in the above toughness scaling methodology is that parameter m is independent of strength mismatch level, M_y, or, at least, it can be considered a weak function of the mismatch ratio. Since this parameter is connected with the assumed microcrack distribution (see the Appendix), the merits of such an assumption are questionable. Indeed, different weld materials would plausibly exhibit different microcrack distributions thereby affecting the m-value for each material. However, in using the present scaling model in the sense of asking whether parameter m will or will not remain a material property, it should be kept in mind the predictive nature and the engineering character of the proposed framework. For low to moderate levels of weld overmatch ($M_y \leq 1.2$–1.3), the adopted assumption appears consistent with the development pursued in this work while, at the same time, maintaining the relative simplicity of the TSM to welded components given current knowledge. For the present, this issue is considered unresolved and the analyses proceed based upon the weak dependence of parameter m on strength mismatch level. As will be discussed later in Sect. 6.3, the adopted engineering procedure is rather effective in predicting the failure strain of a 10% overmatch wide plate specimen even though its level of crack-tip constraint varies widely from a conventional, laboratory fracture specimen under bending. Experimental work to address the potential dependence of parameter m on strength mismatch along with additional verification analyses is currently in progress.

2.3 Weibull modulus calibration

Application of the methodology outlined above requires correct specification of the m-value entering directly into the calculation of σ_w through Eq. (3) thereby enabling evaluation of $\bar{\sigma}_w$. This parameter thus play a crucial role in defining the scaling curves displayed in Fig. 2 upon which the toughness correction is derived. The following steps summarize the key procedures in the calibration of parameter m based upon $\bar{\sigma}_w$-based scaling curves to correct toughness values for effects of weld strength mismatch derived from two data sets. The approach builds upon previous calibration strategy for homogeneous materials introduced by Gao et al. (1998) and Ruggieri et al. (2000), and remains applicable for other macroscopic measures of loading, such as CTOD. The next sections illustrate a validation study of the process for an API X80 girth weld.

- *Step 1*
  Test two sets of specimens with different strength mismatch conditions (**A** and **B**) in the ductile-to-brittle transition region to generate two distributions of fracture toughness data. Ideally, configuration **A** should correspond to fracture specimens for the evenmatch condition ($M_y = 1$). Determine the characteristic toughness value for each data set, J_0^A and J_0^B, using a standard maximum likelihood estimation procedure (Mann et al. 1974). Alternatively, the Master Curve procedure given by ASTM E-1921 (American Society for Testing and Materials 2008b) can be employed with the fracture toughness measure, K_{Jc}, replaced by J_c which enables defining J_0 in the form

$$J_0 = \left[\frac{1}{N_J} \sum_{k=1}^{N_J} J_{c,k}^2 \right]^{1/2} \tag{8}$$

  where N_J is the number of tested specimens for each crack configuration. In the above formulation, it is understood that the threshold fracture toughness, $J_{\min}$, is set equal to zero and the Weibull modulus, α, of the corresponding Weibull distribution is assigned a fixed value of 2. Select the specimen geometries, mismatch conditions and the common test temperature to insure different evolutions of σ_w levels for the two configurations. No ductile tearing should develop prior to cleavage fracture in either sets of tests. In case limited ductile tearing does develop in some specimens, the corresponding toughness values can be treated as censored values by manipulating the Master Curve procedure as above (see ASTM E-1921 (2008b)) in the form

$$J_0 = \left[\frac{1}{r} \sum_{k=1}^{N_J} J_{c,k}^2 \right]^{1/2} \tag{9}$$

  where r is now the number of tested specimens exhibiting no ductile tearing.
- *Step 2*
  Perform detailed, nonlinear finite element analyses in large geometry change (LGC) setting for the tested specimen geometries. The mesh refinements

must be sufficient to insure converged σ_w versus J (or $\bar{\sigma}_w$ versus $\bar{J}$) histories for the expected range of m-values and loading levels.

- *Step 3*

  3.1 Assume an m-value. Compute the $\bar{\sigma}_w$ versus $\bar{J}$ trajectories for configurations **A** and **B** to construct the toughness scaling model relative to both configurations.

  3.2 Correct $\bar{J}_0^A$ to its equivalent $\bar{J}_0^B$, i.e., the corrected value of the mean toughness for the assumed m-value for effects of weld strength mismatch. Define the error of toughness scaling as $R(m) = \left(\bar{J}_{0,m}^A - \bar{J}_0^A\right)/\bar{J}_0^A$.

  3.3 If $R(m) \neq 0$, repeat substeps 3.1–3.2 for additional m-values. The calibrated Weibull modulus, $m = m_0$, makes $R(m) = 0$ within a small tolerance.

3 Description of constraint in mismatched welds: *J*-*Q* approach

For a given specimen geometry or crack configuration, mismatch between the weld metal and base plate strength strongly affects the coupling relationship between J (CTOD) and the near-tip stress fields. Under large-scale yielding and increased loads in overmatched welds, the crack tip plastic zones increasingly spread across the entire weld metal along a large spatial extent well into the base metal. Under such conditions, stresses change from the values determined uniquely by the J-integral (Anderson 2005) for the high constraint condition of small-scale yielding (SSY) (Hutchinson 1983) that exists early in the loading when near-tip plasticity is well embedded within the weld metal. A strong mismatch dependence of fracture behavior is associated with different levels of crack tip constraint for varying degrees of strength mismatch and specimen or component geometry.

To examine the effects of strength mismatch on crack-tip stress fields, the present work adopts the J–Q methodology developed by O'Dowd and Shih (1991, 1992), hereafter denoted OS, as a convenient description of crack-tip constraint. By employing asymptotic analyses and detailed finite element computations, they proposed an approximate two-parameter description for the elastic-plastic crack tip fields based upon a triaxiality parameter more applicable under large scale yielding (LSY) conditions for materials with elastic-plastic response described by a power hardening law given by $\varepsilon/\varepsilon_{ys} \propto \left(\sigma/\sigma_{ys}\right)^n$. Here, n denotes the strain hardening exponent, σ_{ys} and ε_{ys} are the (reference) yield stress and strain, respectively. Guided by detailed numerical analyses, OS identified a family of difference fields, σ_{diff}, in the form

$$\sigma_{ij} = \left(\sigma_{ij}\right)_{SSY} + \left(\sigma_{ij}\right)_{diff} = \left(\sigma_{ij}\right)_{SSY} + f_{ij}\left(\frac{r}{J/\sigma_{ys}}, \theta, Q\right) \tag{10}$$

where the dimensionless second parameter Q defines the amount by which σ_{ij} in fracture specimens or structural components differ from the adopted reference SSY solution, which is usually associated with an infinite cracked plate. Here r and θ are polar coordinates centered at the crack tip with $\theta = 0$ corresponding to a line ahead of the crack.

Limiting attention to the forward sector ahead of the crack tip between the reference (SSY) and the fracture specimen fields, the quantity $Q\sigma_{ys}$ corresponds effectively to a spatially uniform hydrostatic stress, i.e., the difference field relative to the high triaxiality reference stress state. For Mode I fracture (which is associated with the opening stresses, σ_{yy}), OS defined parameter Q simply as

$$Q = \frac{\sigma_{yy} - \left(\sigma_{yy}\right)_{SSY}}{\sigma_{ys}} \text{ at } r = 2J/\sigma_{ys} \tag{11}$$

where the difference field is evaluated at the microscale distance $r = 2J/\sigma_{ys}$ which represents the location of the triggering cleavage mechanism ahead of the crack tip. Further details on the J-Q methodology can also be found in refs. Cravero and Ruggieri (2005), Silva et al. (2006), Dodds et al. (1993, 1997), Nevalainen and Dodds (1995).

The above framework was developed for homogeneous materials but can extended to a center-cracked weld specimen or component in a straightforward manner. Based upon the interpretation of Q as a measure of the level of stress triaxiality that quantifies the difference field relative to a reference stress state, an alternative form applicable to mismatched welds, denoted as Q_{WM} in the present work, can be defined as

$$Q_{WM} = \frac{\sigma_{yy}^{WM} - \left(\sigma_{yy}^{BM}\right)_{SSY}}{\sigma_{ys}^{WM}} \quad \text{at } r = 2J/\sigma_{ys}^{WM} \tag{12}$$

where the difference field, $\left(\sigma_{yy}^{WM} - \left(\sigma_{yy}^{BM}\right)_{SSY}\right)$, now represents the amount by which the near-tip opening

stresses in the weld metal differ from the adopted SSY reference solution for the base plate with σ_{ys}^{WM} denoting the yield stress for the weld metal. Section 5 addresses application of parameter Q_{WM} to characterize effects of weld strength mismatch on crack-tip constraint for key center-cracked weld configurations.

4 Numerical procedures and computational models

4.1 Finite element models for the fracture specimens

3-D nonlinear finite element analyses are conducted on different welded crack configurations which include: (1) a conventional, plane sided SE(B) specimen with $a/W = 0.5$, $B = 25$ mm, $W = 25$ mm and $S = 4W$ and (2) a clamped surface crack SC(T) specimen with $a/t = 0.24$, $c/a = 8.3$, $t = 25$ mm, $2W = 400$ mm and $L = 300$ mm. For the SE(B) specimens, a is the crack length, W is the specimen width, B is the specimen thickness and S is the bend specimen span. For the SC(T) specimen, a is the maximum depth of the surface crack, $2c$ is the length of the semi-elliptical crack, t is the thickness of the cracked section, $2W$ is the specimen width and L is the specimen length. The weld groove width for both specimen configurations is $2h = 10$ mm. Figure 3 shows the geometry and specimen dimensions for the analyzed crack configurations. Minami et al. (1995) used these specimens to measure the cleavage fracture resistance for steel weldments made of an API X80 pipeline steel as described in Sect. 6.1.

Figure 4a shows the finite element model constructed for the 3-D analyses of the SE(B) specimen. A conventional mesh configuration having a focused ring of elements surrounding the crack front is used with a small key-hole at the crack tip; the radius of the key-hole, ρ_0, is 50 μ mm (0.05 mm). Exploratory numerical analyses reveal that such mesh design, while somewhat coarser than previous studies (Ruggieri and Dodds 1996a,b; Ruggieri 2001), still provides adequate resolution of the near-tip stress-strain fields as required for numerical evaluation of σ_w with increased J-values. Symmetry conditions permit modeling of only one-quarter of the specimen with appropriate constraints imposed on the remaining ligament. The quarter-symmetric, 3-D model has 12 variable thickness layers with ~10,000 8-node, 3D elements (~12,000 nodes) defined over the half-thickness ($B/2$); the thickest layer is defined at $Z = 0$ with thinner layers defined near the free surface ($Z = B/2$) to accommodate strong Z variations in the stress distribution. This finite element model is loaded by displacement increments imposed on the loading points to enhance numerical convergence with increased levels of deformation.

Figure 4b displays the finite element model constructed for the 3-D analyses of the SC(T) specimen. Symmetry conditions enable analyses using one-quarter of the 3-D model with appropriate constraints imposed on the symmetry planes. A focused ring of elements surrounding the crack front in the radial direction is used with a small key-hole at the crack tip; the radius of the key-hole, ρ_0, is also 50 μ mm with similar levels of refinement along the crack front that closely match

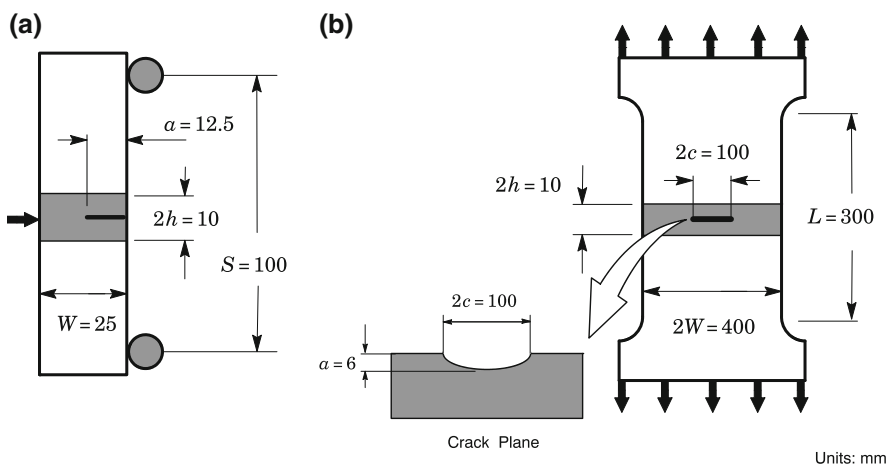

Fig. 3 Geometries for the fracture specimens tested by Minami et al. (1995): **a** SE(B) specimens; **b** Wide Plate SC(T) specimen with a surface center crack

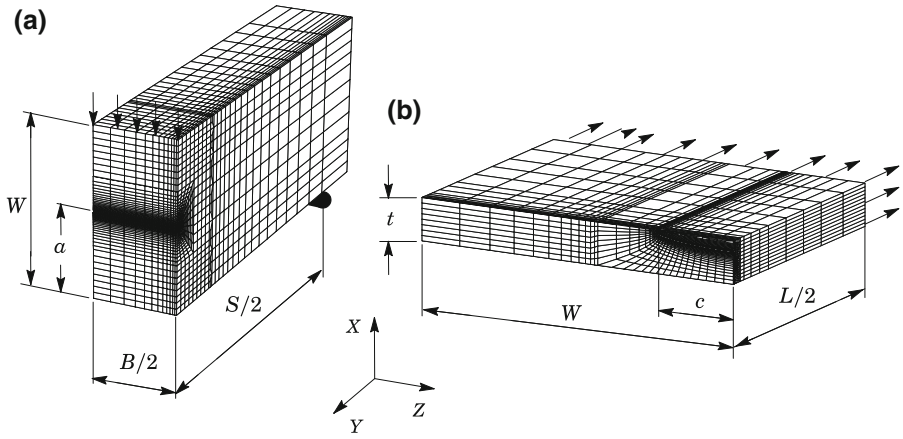

Fig. 4 Finite element models for the specimens employed in the analyses: **a** SE(B) specimens; **b** SC(T) specimen with a surface center crack

the mesh refinement employed in the SE(B) specimen. The half-length of the semi-elliptical crack is defined by 16 elements arranged over the (one-half) crack front. The quarter-symmetric, 3-D model for the SC(T) specimens has ~6,300 8-node, 3D elements (~7,500 nodes). This finite element model is also loaded by displacement increments imposed on the loading points with clamped constraint conditions at the specimen ends.

Nonlinear finite element analyses are also described for plane-strain models of key selected 1-T fracture specimens (which have thickness $B = 25$ mm—see fracture testing terminology standardized by ASTM E1823 (2008a) having a square groove weld with varying weld strength mismatch. These plane-strain models are employed to assess effects of weld strength mismatch on crack-tip constraint based upon the J-Q theory addressed later in Sect. 5. The finite element analyses of these models also provide toughness correction curves based on the Weibull stress for varying mismatch levels. The analysis matrix covers bend and tension loaded fracture specimens with varying geometry and crack sizes: SE(B) with $a/W = 0.2, 0.5$ ($S = 4W$), clamped M(T) with $a/W = 0.5$ ($H = 4W$) and pin-loaded SE(T) with $a/W = 0.5$ ($H = 6W$). Here, a is the crack size (half-crack size for the M(T) specimen), W is the specimen width (half-specimen width for the M(T) specimen) and H is the distance between the pin loading or clamps. All fracture specimens have conventional geometry, i.e., $W = 2B$, with weld groove width, $2h = 15$ mm. Figure 5a shows the geometry and specimen dimensions for the analyzed crack configurations.

Figure 5b shows the finite element model constructed for the plane-strain analyses of the deeply-cracked SE(B) specimen with $a/W = 0.5$ and weld groove width, $2h = 15$ mm. All other crack models have very similar features. Again, a conventional mesh configuration having a focused ring of elements surrounding the crack front is used with a small key-hole at the crack tip; here, the radius of the key-hole, ρ_0, is 10 μ mm (0.01 mm) to enhance computation of J-values at low deformation levels. Symmetry conditions permit modeling of only one-half of the center notch weld specimen with appropriate constraints imposed on the remaining crack ligament. The half-symmetric model has one thickness layer of 1241 8-node, 3-D elements (2678 nodes) with plane-strain constraints imposed ($w = 0$) on each node.

4.2 Computational procedures

The finite element code WARP3D (Gullerud et al. 2004) provides the numerical solutions for the nonlinear computations reported here. The 8-node tri-linear hexahedral elements implemented in WARP3D and used to construct the fracture models incorporate a $\bar{B}$ formulation (Hughes 1980) to alleviate mesh lock-up effects which arise as the deformation progresses into fully plastic modes. The code solves the nonlinear equilibrium equations at each iteration using a very efficient, sparse direct solver highly tuned for Unix and PC-based architectures. This sparse solver significantly reduces both memory and CPU time required for solution of the linearized equations compared to conventional direct solvers. A typical 3-D analysis for solution of the fracture models employed in this study runs in two to 6 hours in a single-processor PC-based workstation.

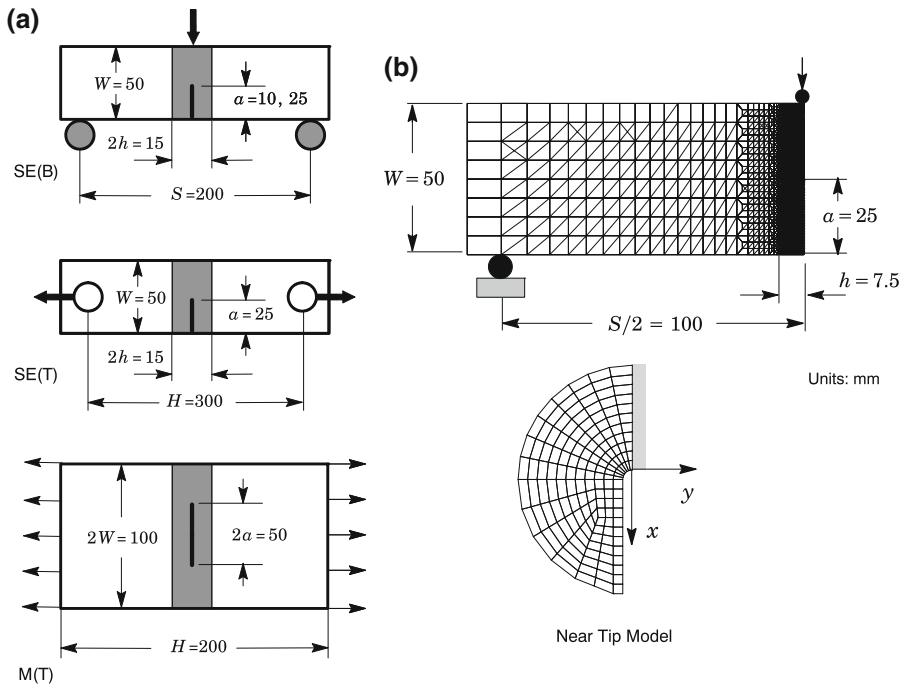

Fig. 5 **a** Geometries for analyzed conventional, 1-T fracture specimens having a center-crack weld; **b** Plane-strain model for the deep notch SE(B) specimen having a center-crack weld

The local value of the mechanical energy release rate at a point s along the crack front is given by Gullerud et al. (2004), Moran and Shih (1987)

$$J(s) = \int_{\Gamma} \left[W_s n_1 - \sigma_{ij} \frac{\partial u_i}{\partial X_1} n_j \right] d\Gamma \tag{13}$$

where Γ denotes a contour defined in a plane normal to the front on the undeformed configuration ($t = 0$) beginning at the bottom crack face and ending on the top face, n_j is the outward normal to Γ, W_s denotes the stress-work density per unit of undeformed volume, σ_{ij} and u_i are Cartesian components of stress and displacement in the crack front coordinate system. The finite element computations employ a domain integral procedure (Moran and Shih 1987) for numerical evaluation of Eq. (13) to provide pointwise values of J across the crack front, J_{local}, and the thickness average value, J_{avg}, at each loading level. For the 3D analyses of the SE(B) specimens, the thickness average values agree well with estimation schemes based upon η-factors for deformation plasticity (Anderson 2005) thus providing a convenient parameter to characterize the average intensity of far field loading on the crack front. For the SC(T) specimens, the intensity of near-tip deformation is quantified by the pointwise value of J evaluated at the point of maximum crack depth (see Fig. 3b). Because the near-tip stress triaxiality is maintained over a large portion of the crack front (Silva et al. 2006) and at distances sufficiently far from the traction-free face of the plate (where the cleavage fracture process has little or negligible significance in the present context), such J-value adequately characterizes the level of crack-tip loading level in the fracture toughness correlations conducted next.

4.3 Finite element form of the generalized Weibull stress

Numerical computations of the Weibull stress used to construct σ_w (or, equivalently, $\bar{\sigma}_w$) versus J trajectories are performed using the research code WSTRESS (Ruggieri 2009a) which implements a finite element form of Beremin's formulation (Beremin 1983). In isoparametric space, the current (deformed) Cartesian coordinates x_i of any point inside a 8-node tri-linear element are related to the parametric coordinates ξ_i using the shape functions corresponding to the k-th node. Let $|\Phi|$ denote the determinant of the standard Jacobian matrix between deformed Cartesian and parametric coordinates. Then using standard procedures for integration over element volumes, the Weibull stress given by previous Eq. (4) has the form

$$\sigma_w = \left[\sum_{N_e} \int_{\Omega_e} \varepsilon_p^{\gamma(1+\beta)} \sigma_1^m d\Omega_e \right]^{1/m} = \left[\sum_{N_e} \int_{-1}^{1} \int_{-1}^{1} \int_{-1}^{1} \varepsilon_p^{\gamma(1+\beta)} \sigma_1^m |\Phi| \, d\xi_1 d\xi_2 d\xi_3 \right]^{1/m} \tag{14}$$

where N_e is the number of elements inside the fracture process zone near the crack tip and Ω_e is the volume of the element. In the above formulation, it is understood that the reference volume, Ω_0, is assigned a unit value, $\Omega_0 = 1$. The process zone used here includes all material inside the loci $\sigma_1 \geq \lambda \sigma_{ys}^{WM}$ with $\lambda = 2$; results for σ_w differ little over a wide range of $\lambda \geq 2$ values. For computational simplicity, an element is included in the fracture process zone if the σ_1 computed at $\xi_1 = \xi_2 = \xi_3 = 0$ (the centroid of the element) exceeds $2\sigma_{ys}^{WM}$. In evaluating the above Eq. (14), the principal stress, σ_1, and the plastic strain, ε_p, are taken at the centroid of the element to provide averaged values of these quantities entering into the computations. Moreover, because the SE(B) fracture specimens utilized to calibrate parameter m and the SC(T) specimen employed in toughness predictions have similar levels of mesh refinement at the crack-tip region, computation of Eq. (14) provide consistent σ_w-values with increased deformation levels even though J varies widely for these crack configurations.

4.4 Material models

The elastic-plastic constitutive model employed in the analyses of the fracture specimens tested by Minami et al. (1995) follows a J_2 flow theory with conventional Mises plasticity in large geometry change (LGC) setting. A piecewise linear approximation to the measured tensile response for the material is adopted to generate numerical solutions for these specimens. Section 6.1 provides the tensile and mechanical properties for the analyzed API X80 pipeline steel (base plate and overmatch weld material).

Assessments of strength mismatch effects on crack-tip constraint and toughness corrections for selected weld fracture specimens addressed in Sect. 5 also require nonlinear finite element solutions utilizing the elastic-plastic constitutive model previously described. Here, the numerical solutions employ a simple power-hardening model to characterize the uniaxial true stress ($\bar{\sigma}$) vs. logarithmic strain ($\bar{\varepsilon}$) in the form

$$\frac{\bar{\varepsilon}}{\varepsilon_{ys}} = \frac{\bar{\sigma}}{\sigma_{ys}} \quad \bar{\varepsilon} \leq \varepsilon_{ys}; \quad \frac{\bar{\varepsilon}}{\varepsilon_{ys}} = \left(\frac{\bar{\sigma}}{\sigma_{ys}} \right)^n \quad \bar{\varepsilon} > \varepsilon_{ys} \tag{15}$$

where σ_{ys} and ε_{ys} are the yield stress and strain, and n is the strain hardening exponent.

The finite element analyses consider material flow properties covering a wide range of low-to-moderate strength mismatch: evenmatch and 10, 20 and 30% overmatch ($M_y = 1.0, 1.1, 1.2$ and 1.3—see Eq. 6). The adopted yield stress and hardening properties of the baseplate material are fixed in all analyses and assigned the following properties: $n = 10$ and $\sigma_{ys} = 412\,\text{MPa}$. Table 1 provides the material properties utilized in the numerical analyses of these fracture specimens with square groove welds which also consider Young's modulus, $E = 206\,\text{GPa}$ and Poisson's ratio, $\nu = 0.3$. The strain hardening parameters for the weld metal are estimated from a simple correlation between the yield stress and hardening exponent applicable for typical structural steels: $n = 5$ and $E/\sigma_{ys} = 800$ (high hardening material), $n = 10$ and $E/\sigma_{ys} = 500$ (moderate hardening material), $n = 20$ and $E/\sigma_{ys} = 300$ (low hardening material). These ranges of properties also reflect the upward trend in yield stress with the increase in strain hardening exponent characteristic of ferritic steels. The hardening exponents for the weld metal are given by a simple linear interpolation of the previous adopted values for σ_{ys} and n.

5 Effects of weld strength mismatch on fracture behavior in conventional specimens

Before addressing application of the toughness scaling model based upon the nondimensional Weibull stress, $\bar{\sigma}_w$, to predict cleavage fracture toughness in weldments, it is useful to examine the general effects of weld strength mismatch on the fracture behavior for selected crack configurations which have a direct bearing on the results presented next. The following sections provide key results derived from the numerical analyses of the plane-strain models for the center-cracked welded specimens described previously in terms of J-Q_{WM} trajectories and mismatch correction curves based upon $\bar{\sigma}_w$.

Table 1 Material properties adopted in the analyses of the 1-T welded fracture specimens

Mismatch level	Weld σ_{ys} (MPa)	n	Baseplate σ_{ys} (Mpa)	n
10% Overmatch	453	11.4	412	10
20% Overmatch	494	12.8	412	10
30% Overmatch	536	14.2	412	10
Evenmatch	412	10	412	10

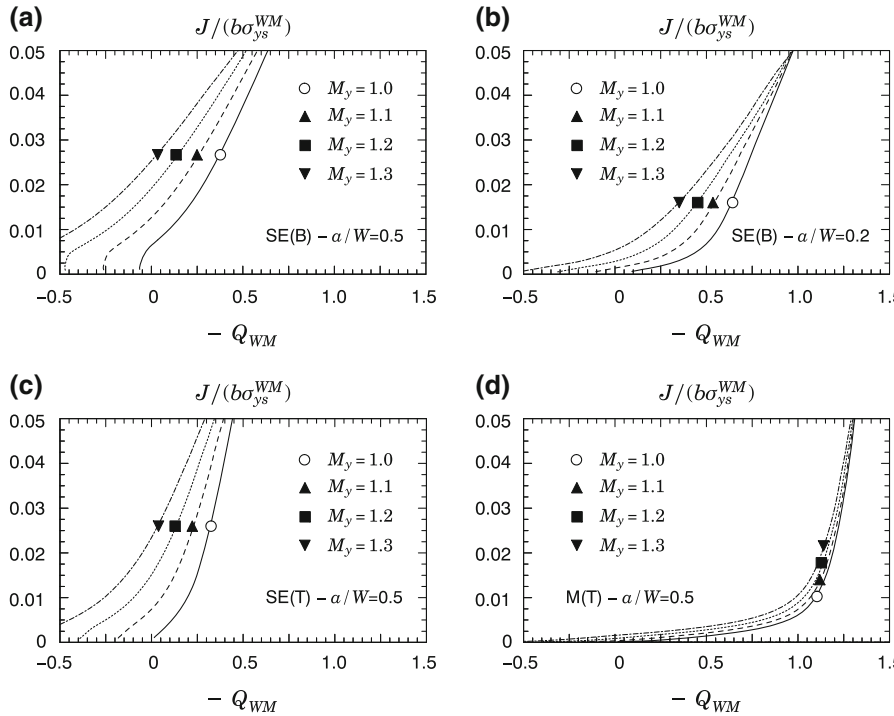

Fig. 6 J-Q_{WM} trajectories for the center-crack weld specimens with varying mismatch ratios

5.1 J-Q_{WM} trajectories for mismatched weld specimens

Figure 6a–d provides descriptions of crack-tip constraint in terms of J-Q_{WM} trajectories for the analyzed welded fracture specimens with varying levels of strength mismatch: evenmatch and 10, 20 and 30% overmatch ($M_y = 1.0, 1.1, 1.2$ and 1.3). Under increased loading, each cracked configuration follows a characteristic J-Q_{WM} trajectory which enables comparison of the corresponding driving force curve in the present context. In all plots, Q_{WM} is defined by Eq. (12) at the normalized distance ahead of crack tip given by $r = 2J/\sigma_{ys}^{WM}$ whereas J is normalized by $b\sigma_{ys}^{WM}$ with b denoting the remaining crack ligament $(W - a)$; to maintain positive scales, Fig. 6 presents plots of $J/b\sigma_{ys}^{WM}$ versus $-Q_{WM}$. The research code FRACTUS2D (Ruggieri 2009b) is employed to compute J-Q_{WM} curves for each fracture specimen.

Consider first the solid curves in each plot describing the evenmatch condition ($M_y = 1.0$) which correspond to the baseplate material with $n = 10$ and $\sigma_{ys} = 412$ MPa; here, $Q_{WM} \equiv Q$. The evolution of Q_{WM} as loading progresses for all analyzed cases depends markedly on the specimen geometry. The deep notch SE(B) and SE(T) specimens display a similar behavior with relatively high levels of stress triaxiality and comparable J-Q_{WM} trajectories for almost the entire range of loading. In contrast, the shallow notch SE(B) and M(T) specimen display much lower levels of stress triaxiality. In particular, the M(T) configuration exhibits its large negative Q_{WM}-values almost immediately upon loading. Here, values for parameter Q_{WM} ranging from -0.75 to -1.25 are associated with substantial

reduction in the opening near-tip stresses for this specimen early in the loading. These findings are fully in accord with previous work of Cravero and Ruggieri (2005) and Nevalainen and Dodds (1995) among others.

Consider now the J-Q_{WM} trajectories with increased levels of weld strength overmatch ($M_y = 1.1$, 1.2 and 1.3) for all fracture specimens. Clearly, a rather strong effect of strength mismatch on fracture behavior is evidenced in these specimens. As expected, strength overmatch increases near-tip stress triaxiality and shifts the curves of J versus Q_{WM} to the left in all plots. Within the present context, such behavior results from an increase in crack-tip constraint (and consequent elevation in near-tip stresses) due to increased levels of weld strength overmatch.

One salient feature emerging from the results displayed in Fig. 6 is the evident coupling behavior between specimen geometry and strength mismatch level. For the high constraint, deeply cracked SE(B) and SE(T) specimens, the J-Q_{WM} curves are strongly sensitive to mismatch ratio; here, the trajectories of J versus Q_{WM} approximately scale with increased M_y-levels. In contrast, the J-Q_{WM} trajectories for the low constraint fracture specimens depend weakly on the M_y-ratio. In particular, parameter Q_{WM} at a given J-value for the M(T) specimen is almost unchanged with increased levels of strength mismatch.

5.2 Toughness correction curves for mismatched Weld Specimens

Figure 7a–d provides the toughness correction curves for the deep and shallow SE(B) specimens ($J_{Even} \rightarrow J_{Over}$ correction) for the 10 and 20% overmatched welds ($M_y = 1.1, 1.2$) with varying Weibull moduli, m. The present computations consider values of $m = 5, 10, 15$ and 20 to assess the sensitivity of the J corrections on the specified Weibull modulus. These m-values are consistent with previously reported values for structural steels (Beremin 1983; Ruggieri and Dodds 1996a,b; Ruggieri 2001, 2009a; Bakker and Koers 1991; Gao et al. 1998; Ruggieri et al. 2000; Gao et al. 1999). Each curve provides pairs of J-values, J_{Even} for the baseplate SE(B) specimen (evenmatch condition with $M_y = 1.0$) and J_{Over} for the overmatch SE(B) specimen, that produce the same $\bar{\sigma}_w$ (see Fig. 2). A reference line is shown which defines a unit ratio of applied J-values in the evenmatch and overmatch SE(B) specimens, i.e., $J_{Even} = J_{Over}$.

These analyses clearly reveal a strong influence of weld strength mismatch on the toughness correction curves displayed in the plots, particularly for the deeply notched bend specimen. The shielding effect of weld overmatch is amply demonstrated by the results shown in Figs. 7a–b as increasing the level of overmatch from 10 to 20% gives rise to an increase in weld toughness, J_{Over}, for a given value of baseplate toughness, J_{Even}. The Weibull modulus, m, does have an appreciable effect on the toughness corrections for this specimen; increasing the m values raises the toughness ratio given by J_{Over}/J_{Even}. In contrast, the toughness correction curves for the shallow notch SE(B) specimen display a somewhat different behavior. Here, the J_{Over}/J_{Even}-ratios for both mismatch levels display less sensitivity to the Weibull modulus with increased values of parameter m.

Much of this J_{Even} versus J_{Over} behavior can be understood in terms of the level of crack-tip constraint and associated near-tip stresses that develop in the weld specimens which affect evolution of the Weibull stress with increased load levels (as characterized by J) in the present context. Consider first the deeply notched SE(B) specimen. For a given load level, weld strength overmatch steadily increases crack-tip constraint for this crack configuration as shown in previous Fig. 6a. Consequently, changes in crack-tip constraint translates almost directly into corresponding changes of the J_{Over}/J_{Even}-ratio for distinct values of parameter m. The results also indicate a gradual saturation in the toughness correction for the 20% overmatch and large m-values, which derives from the higher near-tip stresses that develop in this weld specimen (recall that larger m values assign a greater weight factor to stresses at locations very near the crack front—see Eq. 4). Consider now the shallow notched SE(B) specimen. While the results for this specimen appear consistent with the crack-tip constraint variation exhibited in previous Fig. 6b, changes in the toughness ratios for the 20% overmatch are little insensitive to parameter m in the range $5 \leq m \leq 15$. In this specimen, the severe loss of crack-tip constraint associated with geometry effects offsets the increase in near-tip stress triaxiality due to effects of weld mismatch. In related work to characterize effects of weld strength mismatch on crack driving forces, Donato et al. (2009) showed that intense deformation zones occur outside the near-tip

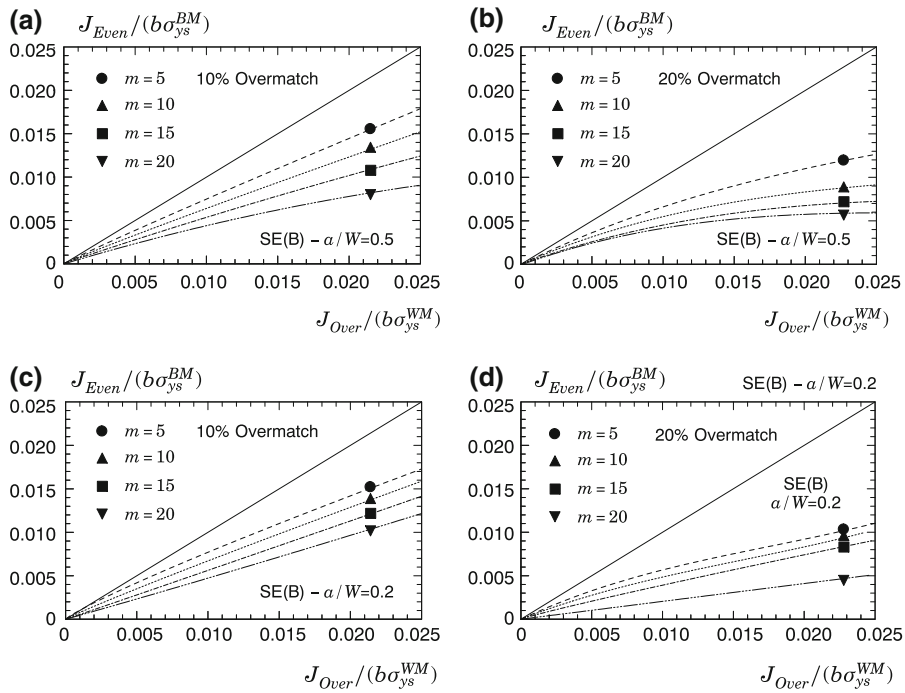

Fig. 7 Toughness correction curves for the deep and shallow notch SE(B) specimens having a center-crack weld and varying Weibull moduli

region close to interface between the weld metal and baseplate material. Such behavior affects computation of the Weibull stress at the crack tip thereby suppressing a more distinct influence of parameter m on toughness corrections.

The above observations taken together also indicate a strong coupling between strength mismatch and specimen geometry that potentially impacts toughness corrections derived from $\bar{\sigma}_w$. Given the interpretation of $\bar{\sigma}_w$ as a macroscopic crack driving force, this feature may introduce additional difficulties in the calibration procedure for parameter m when using low constraint crack configurations. These analyses would then support the adoption of deeply cracked, high constraint weld fracture specimens in calibration procedures of the Weibull modulus as addressed next.

6 Prediction of failure load in girth welds

6.1 Experimental program

Minami et al. (1995) reported on a series of fracture tests conducted on weld specimens made of an API X80 pipeline steel. The welding procedure and welding conditions follow closely those employed in girth welds made in field conditions. Figure 3 shows the tested weld configurations which include deeply notched SE(B) fracture specimens and a wide plate SC(T) specimen with a semi-elliptical, surface center crack with varying levels of weld strength mismatch: evenmatch ($M_y = 1.02$) and 10% overmatch ($M_y = 1.09$). The SE(B) specimens have $a/W = 0.5$ with thickness $B = 25$ mm, width $W = 25$ mm and span distance $S = 100$ mm (refer to Fig. 3). The wide plate specimens have thickness $t = 25$ mm, width $2W$ =400 mm and length $L = 300$ mm; here, the surface crack has length $2c = 100$ mm and depth $a = 6$ mm ($a/t = 0.24$ and $c/a = 8.3$). In all fracture specimens, the weld groove width, $2h$, is 10 mm.

The material is a high strength, low alloy (HSLA) Grade 550 pipeline steel equivalent to an API 5L Grade X80 steel (American Petroleum Institute 2007b). The weld specimens were prepared using standard GMAW procedure with heat inputs ranging from 0.3 to 0.9 kJ/mm according to the pass sequence (see details in Minami et al. 1995). Mechanical tensile tests extracted from the longitudinal weld direction provide the stress-strain data at room (20°C) and test temperature (−5°C). At room temperature, the evenmatch weld has 581 MPa yield stress (σ_{ys}) and 670 MPa tensile strength (σ_{uts}). The 10% overmatch weld has yield stress, $\sigma_{ys} = 621$ MPa, and tensile strength, $\sigma_{uts} = 691$ MPa. The degree of weld strength mismatch at test

temperature is essentially similar to the mismatch level at room temperature. Moreover, both materials display relatively low strain hardening ($\sigma_{uts}/\sigma_{ys} \approx 1.11$–$1.15$) so that effects of hardening mismatch are considered negligible. Other mechanical properties for this material include Young's modulus, $E = 206$ GPa and Poisson's ratio, $\nu = 0.3$. Minami et al. (1995) provide further details on the mechanical tensile test data for this material and describe the uniaxial true stress versus logarithm strain curves at the test temperature, $T = -5°$; these curves were used in the finite element computations reported here.

Testing of the SE(B) specimens was performed at $-5°$C which is within the range of the ductile-to-brittle transition behavior for the material. Records of load versus crack mouth opening displacements (CMOD) were obtained for each specimen using a clip gauge mounted on knife edges attached to the specimen surface. Post-test examinations established the amount of stable crack growth prior to final fracture by cleavage. While Minami et al. (1995) report CTOD toughness values derived from the plastic hinge model using the BS 7448 standard (British Standard 1991), the present analyses are conducted based upon J_c-values. Using the measured plastic work defined by the plastic component of the area under the load versus CMOD curve, the experimental fracture toughness values (J_c) are obtained using the *eta* method (Anderson 2005) with the η-factors given by Donato et al. (2009) for welded SE(B) specimens with center crack grooves and varying tensile properties and mismatch levels. Figure 8a shows the effect of strength mismatch on the measured J_c-values. The toughness values for the 10% overmatch specimens exceed the evenmatch toughness by a factor of 1.5–2.0. Figure 8b provides a Weibull diagram of the measured toughness values for both sets of data. The solid symbols in the plots indicate the experimental fracture toughness data for the specimens. Values of cumulative probability, F_i, are obtained by ordering the J_c-values and using $F_i = (i - 0.3)/(N_J + 4))$, where i denotes the rank number and N_J defines the total number of experimental toughness values. The straight lines indicate the two-parameter Weibull distribution, Eq. (1) with $J_{\min} = 0$, obtained by a maximum likelihood analysis (Mann et al. 1974) of the data set with a fixed Weibull slope of $\alpha = 2$. While the toughness data for the evenmatch specimen agree well with the assumed Weibull distribution, the experimental J_c-values in the low-toughness range for the overmatch specimen deviate from the theoretical slope of $\alpha = 2$. However, the J_0-values (the toughness values corresponding to 63.2% failure probability) needed to perform the calibration procedure described next are essentially unchanged whether the theoretical or the actual statistical distribution is used. This issue is further addressed in the next section.

Fracture testing was also conducted on the wide plate specimens with a 10% overmatch girth weld at $-5°$C. Records of overall (remote) strain, ε_r, versus crack mouth opening displacements (CMOD) were obtained using 4 strain gages conveniently attached at a distance of 100 mm from the notch on both sides of the plate. The specimen failed by overload fracture after some amount of ductile tearing; here, the experimentally measured failure strain (average of the strain gage readings) is given by $\varepsilon_f = 2.25\%$ (Minami et al. 1995).

6.2 Calibration of the Weibull modulus for the tested weldment

The parameter calibration scheme described in Sect. 3 is applied to determine the Weibull modulus for the tested weldment. In the present application, calibration of parameter m is conducted by scaling the mean value of the measured toughness distribution for the evenmatch SE(B) specimen (taken here as the "baseline" value) to an equivalent mean value of the toughness distribution for the 10% overmatch SE(B) specimen. The calibration process simply becomes one of determining an m-value that corrects the nondimensional characteristic toughness value for the evenmatch specimen, denoted $\bar{J}^{Even}_{0,SE(B)}$, to its equivalent value for overmatch specimen, $\bar{J}^{Over}_{0,SE(B)}$. As discussed before in previous Sect. 4.2, use of high constraint deeply cracked SE(B) specimens with different mismatch levels provide toughness correction curves which are very sensitive to parameter m. Consequently, the calibrated Weibull modulus derived from these specimen configurations appears robust enough for subsequent applications. The research code WSTRESS (Ruggieri 2009a) is used to construct $\bar{\sigma}_w$ vs. $\bar{J}$ trajectories for these fracture specimens needed to perform the calibration of parameter m.

As further refinement, the procedure also considers the influence of the plastic strain correction on the Weibull stress and, consequently, on the calibrated Weibull modulus for the tested material using the

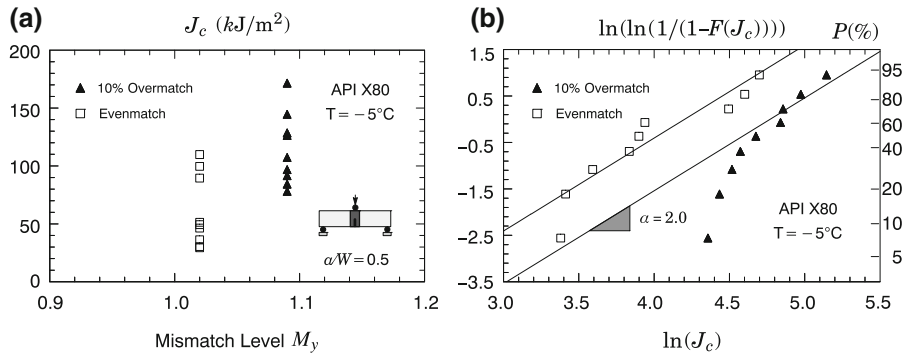

Fig. 8 **a** Experimental toughness values for welded deep crack SE(B) fracture specimens of API X80 steel with two mismatch levels tested by Minami et al. (1995) ($T = -5°$); **b** Weibull distribution of toughness values for the experimental data set of the SE(B) fracture specimens

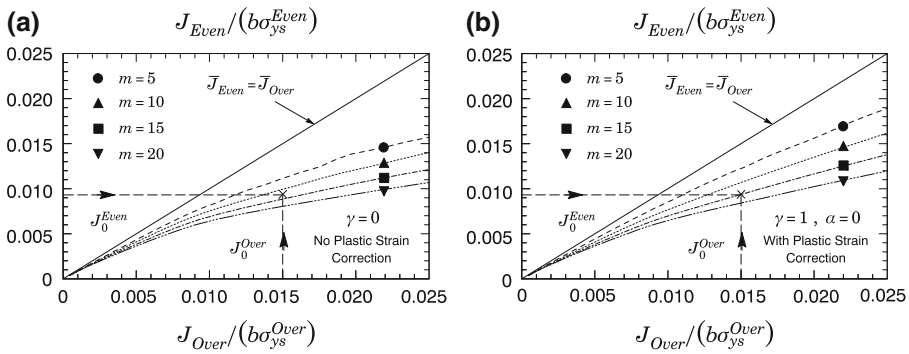

Fig. 9 Toughness correction using the TSM methodology based upon the nondimensional Weibull stress, $\bar{\sigma}_w$, with varying Weibull moduli for the tested welded SE(B) fracture speicmens

generalized definition of previously introduced (see also the Appendix). For the purpose of assessing the effectiveness of Eq. (3) in predictions of the failure strain for the wide plated conducted next, the present investigation considers two sets of widely different parameters defining the microcrack density (see Eq. A.5): i) $\gamma = 0$ (no plastic strain correction) and ii) $\gamma = 1$ and $\beta = 0$ which implies a simple linear dependence of microcrack density on the plastic strain. A similar approach along this line using a linear function for the plastic strain correction has also been pursued by Gao et al. (2005). While this choice of parameters γ and β is somewhat arbitrary, it does make contact with the experimental findings of Lindley et al. (1970) and Gurland (1972) in ferritic steels. Moreover, to go beyond these adopted plastic strain correction parameters, a more detailed microstructural examination would be required which is clearly beyond the scope of this work. Alternatively, a calibration procedure taken into account the effect of plastic strain on cleavage fracture proposed by Beremin (1983) could also be employed. Their approach relies on the testing of notch round tensile specimens which, unfortunately, is not available for the tested material. For the present, the analyses then proceed with the previously adopted plastic strain correction parameters.

Very detailed finite element computations of these specimens enable construction of the $\bar{J}_{0,SE(B)}^{Even} \rightarrow \bar{J}_{0,SE(B)}^{Over}$ correction shown in Fig. 9a–b for varying m-values. In both plots, each curve provides pairs of J-values corresponding to the 10% overmatch and evenmatch SE(B) specimen that produce the same nondimensional σ_w. The Weibull modulus does affect predictions of mismatch effects; here, changing the m-value assigns a different weight factor to stresses at locations very near to the crack front thereby altering the ratio of mismatch correction. A closer inspection of these plots also reveals that the toughness scaling curves for the fracture specimens and mismatch levels considered display only a weak dependence on the adopted plastic strain correction. Because the crack geometry and degree of mismatch for both fracture specimens do not differ significantly, this behavior is not unexpected since the near-tip strain fields for both the evenmatch and overmatch specimens under analysis should be relatively similar.

The calibration scheme now proceeds by adopting a two-parameter Weibull function given by Eq. (1) with

Table 2 Maximum likelihood estimate and corresponding 90% confidence bounds for the two-parameter Weibull distribution of the toughness values measured using the SE(B) fracture specimens

Data set	Theoretical fitting		Actual fitting	
	α	J_0 (kJ/m^2)	α	J_0 (kJ/m^2)
Evenmatch	2.0	66.9 (47.4, 95.8)	2.2	68.4 (50.3, 94.3)
10% Overmatch	2.0	118.0 (83.5, 168.8)	4.2	125.7 (106.9, 149.3)

$\alpha = 2$ and $J_{\min} = 0$ to describe the toughness distribution. Table 2 provides the maximum likelihood estimates (Mann et al. 1974) and the corresponding 90% confidence bounds for parameter J_0 based upon standard distributions of the maximum likelihood estimates given by Thoman et al. (1969). For comparison purposes, Table 2 also includes the maximum likelihood estimates of J_0 relative to the actual distribution ($\alpha \neq 2$). Clearly, setting the Weibull modulus as the theoretical value of $\alpha = 2$ does not alter significantly the estimated J_0-value even though the slope of the fitted distribution for the overmatch data set display a rather large deviation. Once the J_0-values for each mismatch condition is determined, the calibration procedure then yields the Weibull modulus of the tested material at $T = -5°C$ for the two cases considered in the present study: i) $m_0 = 13.5$ for $\gamma = 0$ (no plastic strain correction) and ii) $m_0 = 15.0$ for $\gamma = 1$ and $\beta = 0$ (linear plastic strain correction). Figure 9 recasts the calibration strategy into a graphical procedure for both cases considered to determine parameter m using the scaling curves displayed in that plot. Again, these calibrated m-values are similar and exhibit a relatively minor dependence on the adopted plastic strain correction.

6.3 Prediction of failure strain for the wide plate girth weld

To verify the predictive capability of the Weibull stress methodology adopted in the present work, this section describes application of the toughness scaling model based on the nondimensional Weibull stress ($\bar{\sigma}_w$) incorporating effects of weld strength mismatch and plastic strain to predict the failure strain for the clamped surface crack SC(T) specimen with 10% overmatch. Very detailed nonlinear finite element analyses provide the crack front stress fields to generate the evolution of $\bar{\sigma}_w$ versus $\bar{J}$ for the m-values calibrated in the previous section. Here, the J-value at failure for the tested SC(T) specimen, $\bar{J}^{Over}_{0,SC(T)}$, and the corresponding failure strain are predicted using the measured deep crack toughness values for the evenmatched SE(B) specimen translated in terms of the (nondimensional) characteristic toughness, $\bar{J}^{Even}_{0,SE(B)}$.

Figure 10a–b shows the computed evolution of $\bar{\sigma}_w$ under increasing values of $\bar{J}$ for the SE(B) and SC(T) configurations using the plastic strain correction model with the calibrated m-values. Figure 11 displays the mechanical response of the SC(T) specimen characterized in terms of the evolution of remote applied strain, ε_r, with increased (nondimensional) crack-tip loading, $\bar{J}$. These curves provide the quantitative basis to predict the failure strain for the surface crack specimen with 10% overmatch. Here, because the crack front length of the SC(T) specimen is 4 times the crack front length of the SE(B) specimen (Weisstein), the $\bar{\sigma}_w$-values for the bend specimen must be scaled to the length of the semi-elliptical crack front for the wide plate specimen to guarantee that similar volumes of the (near-tip) fracture process zone are included into the computation of the Weibull stress for each crack configuration (see Eq. 3).

Using again the TSM procedure outline previously, prediction of the failure strain for the SC(T) specimen proceeds as follows. First, the characteristic $\bar{J}_0$-value for the 10% overmatch SC(T) specimen is determined based upon the $\bar{J}_0$-value for the evenmatch SE(B) specimen. The failure strain is then evaluated by means of the computed strain-crack driving force relationship for the wide plate specimen. As a further refinement, the 90% confidence limits for the $\bar{J}_0$-value of the evenmatch SE(B) specimen are also employed to estimate the corresponding 90% confidence bounds for the failure strain of the SC(T) specimen.

Consider first the nondimensional Weibull stress trajectories with no plastic strain correction displayed in Fig. 10a. While $\bar{\sigma}_w$ for the evenmatch SE(B) specimen shows a marked increase with $\bar{J}$, the Weibull stress for the SC(T) specimen rises at a much lower

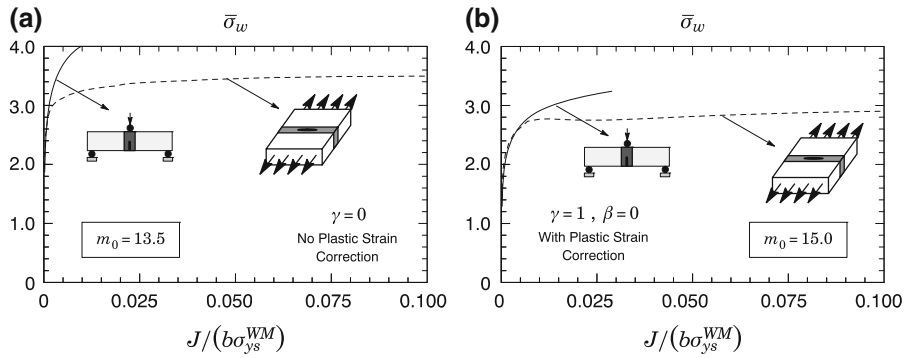

Fig. 10 Nondimensional Weibull stress, $\bar{\sigma}_w$, trajectories with nondimensional J for the evenmatch SE(B) and the overmatch SC(T) specimen for the calibrated m-values

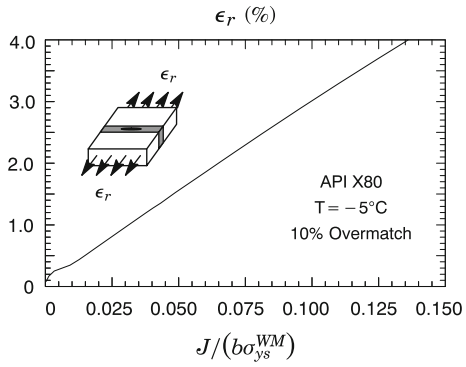

Fig. 11 Evolution of remote applied strain, ε_r, with increased nondimensional J for overmatch SC(T) specimen

rate with increased levels of crack-tip loading. Given the expected toughness ratio $\left(\bar{J}^{Even}_{0,SE(B)}/\bar{J}^{Over}_{0,SC(T)}\right)$ of ≈10–15 for these two data sets (see Fig. 11), the analysis clearly fails to predict the failure strain for the SC(T) specimen. Consider now the evolution of $\bar{\sigma}_w$ versus $\bar{J}$ incorporating the effect of plastic strain displayed in Fig. 10b. With the introduction of the adopted plastic strain correction, a different picture now emerges which can be summarized as follows: 1) The $\bar{\sigma}_w$ vs. $\bar{J}$ trajectory for the evenmatch SE(B) specimen increases rapidly in the initial stage of crack-tip deformation and then more slowly as crack-tip deformation continues and; 2) The overmatch SC(T) specimen also displays a slowly rising Weibull stress curve but which is now fully consistent with the toughness ratio for the analyzed data sets. Table 3 provides the predicted failure strain and corresponding 90% confidence bounds for the wide plate specimen based upon the scaling curve incorporating the plastic strain correction and the plot of ε_r versus $\bar{J}$ displayed in Fig. 11. Even though Minami et al. (1995) report only a single value for the

Table 3 Predicted failure strain and corresponding 90% confidence bounds for the overmatch SC(T) specimen

ε_f	ε_{pred}	90% Bounds	$\varepsilon_{pred}/\varepsilon_f$
0.0225	0.0227	(0.0120, 0.0360)	1.01

experimental failure strain, the ability of the present model in describing the fracture behavior for the overmatch SC(T) specimen seems evident as the predicted failure strain and the 90% confidence bounds agree very well with the experimental data.

7 Summary and concluding remarks

This study describes a probabilistic framework based on the Weibull stress model to predict the effects of weld strength mismatch on macroscopic measures of cleavage fracture toughness applicable to weldments in the ductile-to-brittle transition region. The central feature of this methodology lies on the interpretation of a nondimensional Weibull stress, $\bar{\sigma}_w$, as the crack tip driving force coupled with the simple axiom that cleavage fracture occurs when the nondimensional Weibull stress reaches a critical value, $\bar{\sigma}_{w,c}$. At a fixed temperature, the scaling model requires the attainment of a specified value for $\bar{\sigma}_w$ to trigger cleavage fracture across cracked weld configurations with different mismatch conditions even though the loading parameter (measured by J in the present work) may vary widely due to mismatch and constraint variations. An additional feature of the proposed methodology also includes the effect of near-tip plastic strain on cleavage microcracking which impacts directly the magnitude of the (nondimensional) Weibull stress and, consequently, the toughness scaling correction.

A verification analysis conducted on an overmatch girth weld made of an API X80 pipeline indicates the capability of the micromechanics approach to predict the failure strain for the tested welded component. While rather limited, the analysis results demonstrate the overall effectiveness of the proposed Weibull stress-based criterion using $\bar{\sigma}_w$ in toughness predictions based upon the scaling model. However, for the experimental data set considered here, the preliminary analyses based upon $\bar{\sigma}_w$ computed without the plastic strain correction term failed to predict the experimental failure strain. The introduction of simple set of parameters defining a linear dependence of microcrack density on plastic strain brings the scaling curves to much more consistent levels and produce failure predictions in excellent agreement with the experimental data.

It must be pointed out that the proposed approach is somewhat limited by the proper choice of parameters γ and β defining the plastic strain correction term included into the Weibull stress. Introducing an *ad-hoc* linear dependence of microcrack density on plastic strain in the present model maintains the relative simplicity of the predictive methodology but raises questions about the sensitivity of model predictions to these parameters and underscores the need for additional development of the methodology. Nevertheless, the enormous differences in fracture behavior and crack-tip constraint between the (laboratory) bend specimen and the wide plate component employed in the present study appear to justify this procedure. Overall, the results presented here represent a compelling support to the predictive capability of the Weibull stress methodology in defect assessments of welded components.

Acknowledgments This investigation was supported by the Brazilian Council for Scientific and Technological Development (CNPq). The author greatly acknowledges Prof. F. Minami from Osaka University for making the girth weld data for the API X80 steel available.

Appendix

Probabilistic modeling of cleavage fracture

Incorporating statistics of microcracks

Consider an arbitrarily stressed body where a macroscopic crack lies in a material containing randomly distributed flaws as illustrated in Fig. 1a. The fracture process zone ahead of the crack tip is defined as the highly stressed region where the local operative mechanism for cleavage takes place; this region contains the potential sites for cleavage cracking. For the purpose of developing a probabilistic model for cleavage fracture, divide the fracture process zone ahead of crack tip in N unit volumes statistically independent, $V_i, i = 1, 2, \ldots, N$ subjected to the principal stress σ_1. Each unit volume volume contains a substantially number of statistically independent microflaws uniformly distributed.

The statistical nature of cleavage fracture underlies a simplified treatment for unstable crack propagation of the configuration represented in Fig. 1a based upon weakest link arguments. First limit attention to the asymptotic distribution for failure of the unit volume and consider V divided into small volumes uniformly stressed, statistically independent δV_j, $j = 1, 2, \ldots, n$. Let p denote the probability of failure for the jth volume . The probability that k failures occur (which correspond to the fracture of k small volumes elements) is defined in terms of the Binomial distribution (Feller 1957; Kendall and Stuart 1967)

$$P\left(S_n = k\right) = \binom{n}{k} p^k \left(1 - p\right)^{n-k}, \quad 0 \leq k \leq n, \tag{A.1}$$

where S_n denotes the total number of failures that occurred in n volumes. When k is large and p is small, by the Poisson limit theorem, the distribution of the number of failures converges to a Poisson distribution with parameter μ in the form

$$P\left(S_n = k\right) = \frac{e^{-\mu}\mu^k}{k!}, \tag{A.2}$$

where $\mu = kp$ is the expectation of the binomial distribution. In particular, the probability that at least one failure occurs is sought. Thus, the failure probability of the unit volume, P_0, converges to the distribution (Feller 1957; Kendall and Stuart 1967)

$$P_0 = P\left(S_n \geq 1\right) = 1 - P\left(S_n = 0\right) = 1 - e^{-\mu}. \tag{A.3}$$

To arrive at a limiting distribution for the fracture stress of a cracked solid, an appropriate functional form for the probability p is required. The most widely adopted probabilistic model to describe fracture in brittle materials is based upon the weakest link (WL) theory. A central feature emerging from the WL model is the notion

that catastrophic failure is driven by unstable propagation of a single critical microflaw or microcrack contained in the unit volume V which allows expressing the average number of failures, μ, as

$$\mu = \int_{l_c}^{\infty} g(l)\, dl \tag{A.4}$$

where l is the microcrack size, l_c is the critical microcrack size and g represents the microcrack density function. Here, it is understood that the failure probability p depends on the stress level, σ_1, acting on V, i.e., $p = p(\sigma_1)$. A common assumption adopts an asymptotic distribution for the microcrack density in the form $g(l) = (\psi_0/l)^{\zeta}$ (Beremin 1983; Evans and Langdon 1976; Freudenthal 1968) where ζ and ψ_0 are parameters of the distribution. However, previous fundamental work (Averbach 1965; Tetelman and McEvily 1967) clearly shows the strong effect of plastic deformation, in the form of inhomogeneous arrays of dislocations, on microcrack nucleation which triggers cleavage fracture at the material's microlevel. Based upon direct observations of cleavage microcracking by plastic strain made in ferritic steels at varying temperatures (Brindley 1970; Lindley et al. 1970; Gurland 1972), the microcrack density can then be further generalized in terms of

$$g(l) = \varepsilon_p^{\gamma(1+\beta)} \left(\frac{\psi_0}{l}\right)^{\zeta}, \tag{A.5}$$

where ε_p is the (effective) plastic strain, γ and β represent parameters defining a power law relationship between the microcrack density and plastic strain as inferred in Lindley et al. (1970).

Now, upon introducing the dependence between the critical microcrack size, l_c, and (local) stress in the form $l_c = \left(K_{Ic}^2/Y^2\sigma_1^2\right)$, where Y represents a geometry factor and K_{Ic} is the critical stress intensity factor, and substituting Eq. (A.5) into Eq. (A.4), the mean μ resolves to

$$\mu = \varepsilon_p^{\gamma(1+\beta)} \left(\frac{\sigma_1}{S_0}\right)^m, \tag{A.6}$$

where parameters $m = 2\zeta - 2$ and S_0 are related to the microcrack distribution with m and $S_0 > 0$. Using this result in Eq. (A.3) enables defining the failure probability for the unit volume V in the form

$$\begin{aligned} P_0 &= 1 - \exp\left[-\varepsilon_p^{\gamma(1+\beta)} \left(\frac{\sigma_1}{\sigma_u}\right)^m\right] \\ &= 1 - \exp\left[-\left(\frac{\tilde{\sigma}_1}{\sigma_u}\right)^m\right], \end{aligned} \tag{A.7}$$

which is a Weibull (1939) distribution with parameters m and σ_u.

Further development in the adopted probabilistic framework requires invoking again weakest link arguments to generalize the previous probability distribution to any multiaxially stressed region, such as the fracture process zone ahead of a macroscopic crack or notch (see Fig. 1a). Here, the statistical problem of determining an asymptotic distribution for the fracture strength of the entire solid is equivalent to determining the distribution of the weakest unit volume V. The fundamental assumption is that the near-tip fracture process zone consists of N arbitrary and statistically independent, unit volumes V. Consequently,

$$P = 1 - [1 - P_0]^N = 1 - \prod_{i=1}^{N} (1 - P_0). \tag{A.8}$$

Substituting Eq. (A.7) into the above expression and making $N \to \infty$, the probability distribution of the fracture stress for a cracked solid based upon the WL model is given by

$$P = 1 - \exp\left[-\frac{1}{\Omega_0}\int_{\Omega} \varepsilon_p^{\gamma(1+\beta)} \left(\frac{\sigma_1}{\sigma_u}\right)^m d\Omega\right] \tag{A.9}$$

where Ω denotes the volume of the near-tip fracture process zone and Ω_0 is a reference volume usually taken as unit, i.e., $\Omega_0 = 1$. In the present work, the active fracture process zone is defined as the loci where $\sigma_1 \geq \lambda\sigma_{ys}$ in which $\lambda \approx 2$ and σ_{ys} defines the material's yield stress.

Following the development presented previously, the Beremin (1983) stress is then given by integration of the principal stress over the fracture process zone in the form

$$\sigma_w = \left[\frac{1}{\Omega_0}\int_{\Omega} \varepsilon_p^{\gamma(1+\beta)} \sigma_1^m d\Omega\right]^{1/m} \tag{A.10}$$

from which the probability distribution given by Eq. (A.9) now takes the form

$$P(\sigma_w) = 1 - \exp\left[-\left(\frac{\sigma_w}{\sigma_u}\right)^m\right]. \tag{A.11}$$

Equation (A.11) defines a two-parameter Weibull (1939) distribution for the Weibull stress in terms of the Weibull modulus m and the scale factor σ_u. A central feature of this methodology involves the interpretation of as σ_u a macroscopic crack driving force (Ruggieri and Dodds 1996a,b; Ruggieri 2001, 2009a).

Consequently, it follows that unstable crack propagation (cleavage) occurs at a critical value of the Weibull stress; under increased remote loading (as measured by *J*), differences in evolution of the Weibull stress reflect the potentially strong variations of near-tip stress fields.

References

American Petroleum Institute (2005) Welding of pipelines and related facilities, 20th edn. API 1104

American Petroleum Institute (2007a) Fitness-for-service. API RP-579-1/ASME FFS-1

American Petroleum Institute (2007b) API specification for 5L line pipe, 44th edn

American Society of Mechanical Engineers (2004) Boiler and pressure vessel code. New York

American Society for Testing and Materials (2008a) Standard terminology relating to fatigue and fracture testing. ASTM E-1823, Philadelphia

American Society for Testing and Materials (2008b) Standard test methods for determination of reference temperature, T_0, for ferritic steels in the transition range. ASTM E-1921, Philadelphia

American Welding Society (1987) Welding handbook: welding Technology, 8th edn, vol 1. Miami

Anderson TL (2005) Fracture mechanics: fundaments and applications. 3rd edn. CRC Press, New York

Averbach BL (1965) Micro and macro formation. Int J Fract Mech 1:272–290

Bakker A, Koers RWJ (1991) Prediction of cleavage fracture events in the brittle–ductile transition region of a Ferritic steel. In: Blauel JG, Schwalbe KH (eds) Defect assessment in components—fundamentals and applications, ESIS/EG9. Mechanical Engineering Publications, London pp 613–632

Beremin FM (1983) A local criterion for cleavage fracture of a nuclear pressure vessel steel. Metall Trans 14:2277–2287

Brindley BJ (1970) The effect of dynamic strain-aging on the ductile fracture process in mild steel. Acta Metall 18:325–329

British Standard (1991) Fracture mechanics toughness tests. BS 7448

British Standard Institution (2005) Guide on methods for assessing the acceptability of flaws in metallic structures, BS7910

Cravero S, Ruggieri C (2005) Correlation of fracture behavior in high pressure pipelines with axial flaws using constraint designed test specimens—part I: plane-strain analyses. Eng Fract Mech 72:1344–1360

Det Norske Veritas (2007) Submarine pipeline systems. Offshore Standard OS-F101

Dodds RH, Shih CF, Anderson TL (1993) Continuum and micro-mechanics treatment of constraint in fracture. Int J Fract 64:101–133

Dodds RH, Ruggieri C, Koppenhoefer K (1997) 3-D constraint effects on models for transferability of cleavage fracture toughness. In: Underwood JH (ed) et al Fatigue and fracture mechanics: 28th Volume, ASTM STP 1321. American Society for Testing and Materials, Philadelphia, pp 179–197

Donato GHB, Magnabosco R, Ruggieri C (2009) Effects of weld strength mismatch on *J* and CTOD estimation procedure for SE(B) specimens. Int J Fract 159:1–20

Evans AG, Langdon TG (1976) Structural ceramics. Prog Mater Sci 21:171–441

Feller W (1957) Introduction to probability theory and its application vol I. Wiley, New York

Freudenthal AM (1968) Statistical approach to brittle fracture. In: Liebowitz H (ed) Fracture: an advanced treatise vol II. Academic Press, NY pp 592–619

Gao X, Ruggieri C, Dodds RH (1998) Calibration of Weibull stress parameters using fracture toughness data. Int J Fract 92:175–200

Gao X, Dodds RH, Tregoning RL, Joyce JA, Link RE (1999) A Weibull stress model to predict cleavage fracture in plates containing surface cracks. Fatigue Fract Eng Mater Struct 22:481–493

Gao X, Zhang G, Srivatsan TS (2005) Prediction of cleavage fracture in ferritic steels: a modified Weibull stress model. Mater Sci Eng A 394:210–219

Glover AG, Hauser D, Metzbower EA (1986) Failures of weldments. In: Metals handbook, vol 11: failure analysis and prevention. American Society for Metals, pp 411–449

Gurland J (1972) Observations on the fracture of cementite particles in a spheroidized 1.05% C steel deformed at room temperature. Acta Metall 20:735–741

Gullerud A, Koppenhoefer K, Roy A, RoyChowdhury S, Walters M, Bichon B, Cochran K, Dodds R (2004) WARP3D: dynamic nonlinear fracture analysis of solids using a parallel computers and workstations. Structural Research Series (SRS) 607. UILU-ENG-95-2012. University of Illinois at Urbana-Champaign

Hughes TJ (1980) Generalization of selective integration procedures to anisotropic and nonlinear media. Int J Numer Methods Eng 15:1413–1418

Hutchinson JW (1983) Fundamentals of the phenomenological theory of nonlinear fracture mechanics. J Appl Mech 50:1042–1051

Jutla T (1996) Fatigue and fracture control of weldments. In: ASM handbook, vol 19: fatigue and fracture. ASM International, pp 434–449

Kendall MG, Stuart A (1967) The advanced theory of statistics. 2nd edn. Hafner, New York

Kerr WH (1976) A review of factors affecting toughnness in welded steels. Int J Press Vessel Piping 4:119–141

Lin T, Evans AG, Ritchie RO (1986) A statistical model of brittle fracture by transgranular cleavage. J Mech Phys Solids 21:263–277

Lindley TC, Oates G, Richards CE (1970) A critical appraisal of carbide cracking mechanism in ferride/carbide aggregates. Acta Metall 18:1127–1136

Mann NR, Schafer RE, Singpurwalla ND (1974) Methods for statistical analysis of reliability and life data. Wiley, New York

Matsuo Y (1981) Statistical theory for multiaxial stress states using Weibull's three-parameter function. Eng Fract Mech 14:527–538

Minami F, Brückner-Foit A, Munz D, Trolldenier B (1992) Estimation procedure for the Weibull parameters used in the local approach. Int J Fract 54:197–210

Minami F, Ohata M, Toyoda M, Tanaka T, Arimochi K, Glover AG, North TH (1995) The effect of weld metal yield strength on the fracture behavior of girth welds in grade 550 pipe. Pipeline Technol 1:441–461

Moran B, Shih CF (1987) A general treatment of crack tip contour integrals. Int J Fract 35:295–310

Nevalainen M, Dodds RH (1995) Numerical investigation of 3-D constraint effects on brittle fracture in SE(B) and C(T) specimens. Int J Fract 74:131–161

O'Dowd NP, Shih CF (1991) Family of crack-tip fields characterized by a triaxiality parameter: part I—structure of fields. J Mech Phys Solids 39(8):989–1015

O'Dowd NP, Shih CF (1992) Family of crack-tip fields characterized by a triaxiality parameter: part II—fracture applications. J Mech Phys Solids 40:939–963

Ruggieri C, Dodds RH (1996a) A transferability model for brittle fracture including constraint and ductile tearing effects: a probabilistic approach. Int J Fract 79:309–340

Ruggieri C, Dodds RH (1996b) Probabilistic modeling of brittle fracture including 3-D effects on constraint loss and ductile tearing. J Phys

Ruggieri C (2001) Influence of threshold parameters on cleavage fracture predictions using the Weibull stress model. Int J Fract 110:281–304

Ruggieri C (2009a) WSTRESS release 3.0: numerical computation of probabilistic fracture parameters for 3-D cracked solids. EPUSP, University of São Paulo

Ruggieri C (2009b) FRACTUS2D: numerical computation of fracture mechanics parameters for 2-D cracked solids. EPUSP, University of São Paulo

Ruggieri C, Gao X, Dodds RH (2000) Transferability of elastic-plastic fracture toughness using the Weibull stress approach: significance of parameter calibration. Eng Fract Mech 67:101–117

Silva LAL, Cravero S, Ruggieri C (2006) Correlation of fracture behavior in high pressure pipelines with axial flaws using constraint designed test specimens—part II: 3-D effects on constraint. Eng Fract Mech 73:2123–2138

Tetelman AS, McEvily AJ (1967) Fracture of structural materials. Wiley, New York

Thoman DR, Bain LJ, Antle CE (1969) Inferences on the parameters of the Weibull distribution. Technometrics 11:445–460

Wallin K (1984) The scatter in KIc results. Eng Fract Mech 19:1085–1093

Wallin K (2002) Master curve analysis of the Euro fracture toughness dataset. Eng Fract Mech 69:451–481

Weibull W (1939) The phenomenon of rupture in solids. Ingeniors Vetenskaps Akademien Handl 153:55

Weisstein EW (2009) "Ellipse" in mathWorld—a wolfram web resource. http://www.mathworld.wolfram.com/Ellipse.html